Vertical "III–V" V-Shaped Nanomembranes Epitaxially Grown on a Patterned Si[001] Substrate and Their Enhanced Light Scattering

Sònia Conesa-Boj,[†,¶] Eleonora Russo-Averchi,[†,¶] Anna Dalmau-Mallorqui,[†] Jacob Trevino,[‡] Emanuele F. Pecora,[‡] Carlo Forestiere,[‡,§] Alex Handin,[‡] Martin Ek,[⊥] Ludovit Zweifel,[†] L. Reine Wallenberg,[⊥] Daniel Rüffer,[†] Martin Heiss,[†] David Troadec,[⊥] Luca Dal Negro,[‡] Philippe Caroff,[∥] and Anna Fontcuberta i Morral[†,*]

[†]Laboratoire des Matériaux Semiconducteurs, Ecole Polytechnique Fédérale de Lausanne, 1015 Lausanne, Switzerland, [‡]Department of Electrical and Computer Engineering & Photonics Center, Boston University, 8 Saint Mary Street, Boston, Massachusetts 02215, United States, [§]Department of Electrical Engineering, Università degli Studi di Napoli Federico II, via Claudio 21, Napoli 80125, Italy, [⊥]nCHREM/Polymer & Materials Chemistry, Lund University, Box 124, S-22100 Lund, Sweden, and [∥]Institut d'Electronique, de Microélectronique et de Nanotechnologie, UMR CNRS 8520, Avenue Poincaré, B.P. 60069, 59652 Villeneuve d'Ascq, France. [¶]These authors contributed equally to this work.

ABSTRACT We report on a new form of III–V compound semiconductor nanostructures growing epitaxially as vertical V-shaped nanomembranes on Si(001) and study their light-scattering properties. Precise position control of the InAs nanostructures in regular arrays is demonstrated by bottom-up synthesis using molecular beam epitaxy in nanoscale apertures on a SiO_2 mask. The InAs V-shaped nanomembranes are found to originate from the two opposite facets of a rectangular pyramidal island nucleus and extend along two opposite ⟨111⟩ B directions, forming flat {110} walls. Dark-field scattering experiments, in combination with light-scattering theory, show the presence of distinctive shape-dependent optical resonances significantly enhancing the local intensity of incident electromagnetic fields over tunable spectral regions. These new nanostructures could have interesting potential in nanosensors, infrared light emitters, and nonlinear optical elements.

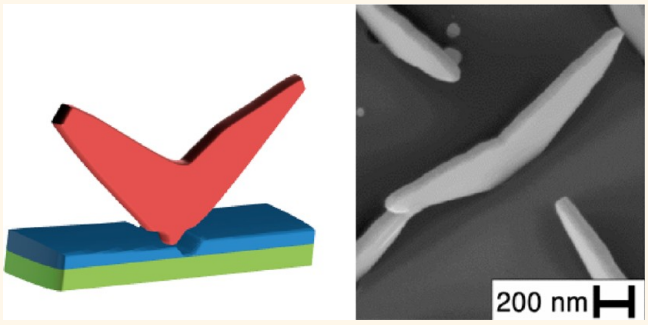

KEYWORDS: III–V nanostructures · nanomembranes · V-shape · nucleation · light scattering

In the last few decades, there has been both in fundamental and applied science a constant effort in reducing the size of semiconductor structures with composition, crystal structure, and morphology controlled down to the nanoscale.[1−3] One of the advantages of nanostructures over traditional thin film technology is the third dimension component resulting in the possibility of reaching complex architectures, impossible by other means. A large variety of shapes have been controllably achieved, spanning from nanomembranes or nanowalls,[4−10] nanotrees,[11] nanoflowers,[12,13] to nanowires.[14−16] Concurrently, nanowires have also enabled three-dimensional hierarchical structures by the formation of tripods,[17] tetrapods,[18] and more generally branched nanostructures.[19−24] This adds a significant versatility from the point of view of material design because these nanostructures can intrinsically integrate p–n junctions and heterostructures such as quantum dots, barriers, and quantum wells.[25,26]

Silicon is the most widely used semiconductor in integrated circuits, while III–V semiconductors are used in optoelectronics and in radio frequency applications, such as digital wireless communications. Most of today's electronics relies on silicon, due to optimal electronic properties and ease of micro-to-nano fabrication. Heterogeneous integration of silicon of III–V compound semiconductors, which have a direct band gap and high carrier mobilities, is thus an exciting challenge as it would lead to a

* Address correspondence to anna.fontcuberta-morral@epfl.ch.

Received for review September 30, 2012 and accepted November 24, 2012.

Published online November 25, 2012
10.1021/nn304526k

combination of the best properties of both semiconductor classes. However, traditional III−V thin film integration on silicon has shown to be extremely challenging due to the lattice, thermal, and polarity mismatches.[27] Free-standing nanoscale structures offer the possibility of epitaxial integration on mismatched group IV substrates. Their small footprint and single nucleation event per nanostructure guarantee an extremely reduced probability for antiphase domain boundary formation and an efficient elastic strain relaxation at the interface—even though the defect density is not zero even for small diameter nanostructures.[28−30]

Several approaches have been investigated for the integration of III−V semiconductors and silicon: heteroepitaxial growth using metalorganic chemical vapor deposition,[31] direct epitaxy (which suffers from lattice and polarity mismatch),[32] growth of a graded SiGe buffer layer for GaAs,[33] and Sb-based metamorphic layers,[34,35,36] wafer bonding,[37,38] and localized epitaxy[39] in nanoscale areas forming nanowires.[40] Recently, gold-free III−V nanowires have been used in high-performance vertically integrated transistors, opening a real perspective for high-performing materials integrated on Si.[41] Additionally, growth achieved on [001]-oriented substrates would bring the integration with current technological processes closer, while at the same time it would result in the reduction of structural defects in nanowires.[42,43] To the best of our knowledge, no example of gold-free vertical III−V nanostructures epitaxially grown on Si(001) has yet been reported. Finally, growth of III−V semiconductors on Si should be obtained in an ordered manner, as this allows for precise positioning of masks and contacts, thus greatly facilitating rational device processing.

In this work, we explore a new form of III−V nanostructures, grown epitaxially on (001) silicon substrates by solid source molecular beam epitaxy (MBE). The nanostructures are self-catalyzed (gold-free) and positioned by means of nanoscale hole arrays created in a thin SiO_2 mask. Surprisingly, we find that instead of nanowires, which were reported for growth on Si(111),[44−48] wing-shaped single-crystalline epitaxial membranes grow perpendicularly to the Si (001) substrates. (While the nanomembranes grow vertically aligned with respect to the substrate, it will be clear from the geometry that its two constituent wings are tilted with respect to the substrate.) We show that the nucleation of these wing-shaped nanostructures originates from an initial nanoscale pyramidal island nucleus. While nucleation occurs in zinc blende phase, the growth of the wings (membranes) occurs mostly in wurtzite phase. Finally, by combining dark-field scattering measurements and light-scattering theory for arbitrarily shaped dielectrics within the accurate surface integral equation (SIE) method,[49] we demonstrate the presence of distinctive shape-dependent optical resonances that can significantly enhance the local intensity of the incident electromagnetic fields over tunable spectral regions. These findings, in combination with the large surface-to-volume ratio offered by these novel dielectric nanostructures, provide a novel approach for the manipulation of nanoscale optical fields and light−matter interactions on a Si substrate, potentially enabling a number of device applications such as enhanced nanosensors, light emitters, and nonlinear optical elements.[50]

RESULTS AND DISCUSSION

General Morphology, Growth Directions, and Epitaxial Relationships. Scanning electron microscopy (SEM) images of the V-shaped membrane structures are shown in Figure 1a−e with various tilt and rotation angles and increasing magnifications from panels c−e. Figure 1a, showing a low-magnification planar view, illustrates the two preferred elongation directions and the vertical feature of the nanostructures, with respect to the substrate. Indeed, after 1 h of growth, membranes between 0.5 and 2 μm long are found to extend along two perpendicular directions in a top-down projection: ⟨1−10⟩ and ⟨110⟩. The membrane thickness shown in the micrographs is about 170 nm, and their flat nanowalls are bound by {110} planes. Overall, depending on the growth conditions and time, the membranes exhibit thicknesses between 50 and 200 nm. The tilted images shown in Figure 1b−e reveal the V-shape of the nanostructures, with arms branching toward two ⟨111⟩ directions. The membranes nucleate in the holes of the SiO_2 mask (see schematic in Figure 1f). To investigate the epitaxial relationship between these nanostructures and the substrate, focused ion beam (FIB)-assisted lamellas were prepared along the ⟨110⟩ and ⟨1−10⟩ directions of the substrate. A low-magnification SEM image of one of these lamellas, prepared for inspection by transmission electron microscopy (TEM), is shown in Figure 1g, illustrating connected nanostructures and part of the Si substrate on which they grew. The cross-sectional lamellas were studied by high-resolution TEM focusing on the InAs/Si interface. The interface region for a single nanowing is shown in Figure 1h and in Figure 1i with lattice fringe resolution. A fast Fourier transform (FFT) was calculated from the image of Figure 1i, confirming the epitaxial relationship and the relaxed mismatch of 11.6% between the membrane and the substrate, as shown in Figure 1j.

An analysis of the merging between two membranes is shown in low- and high-resolution TEM in Figure 1k−m. The fringes from each of the branches as well as the interface can be observed. Interestingly, the branches grow onto each other, forming a triangular island with a defect-free zinc blende phase growing in the (001) direction (see diffractogram in Figure 1n). This island is similar to the one observed in the nucleation stage of the structure, with the only difference being that the size is about 30 times larger. The base is about

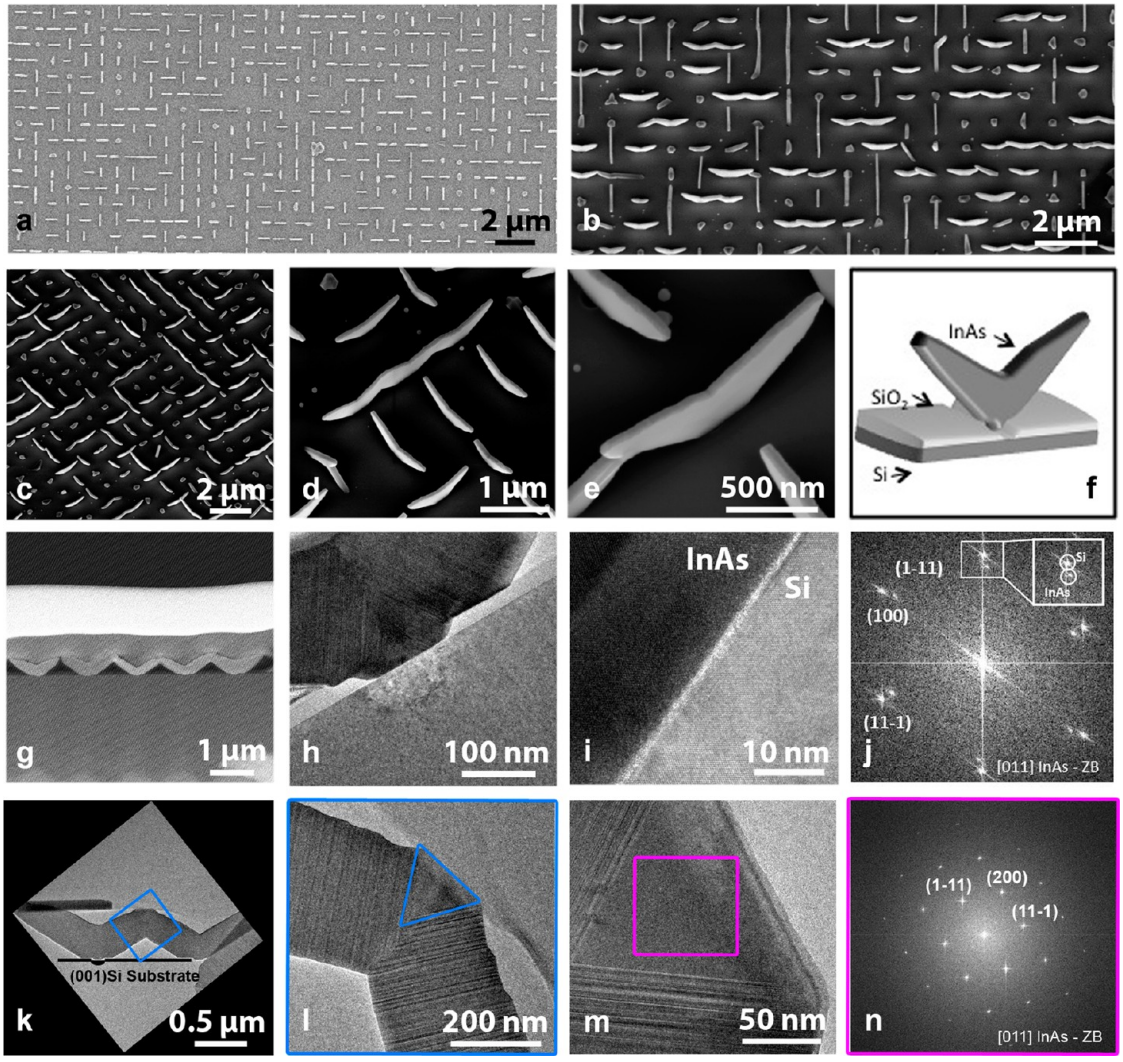

Figure 1. (a−e) Scanning electron microscopy (SEM) images of typical InAs membranes grown at 500 °C under an As_4 partial pressure of 8×10^{-6} Torr. (a) Planar view image, (b) tilted view (30°), and (c−e) tilted views with additional in-plane rotation of 45°. Different scales are presented in order to reveal the intermembrane ordering and the local structure. (f) Schematic of one V-shaped nanomembrane, represented with an oxide mask and substrate. (g) Low-magnification SEM image of a FIB-prepared, perpendicular TEM lamella showing connected wing-shaped nanomembranes. (h) High-resolution TEM image of the nanostructure/silicon interface, with clearly visible contrast probably due to ion-beam-damaged fields in the substrate part. (i) Lattice-fringe-resolved TEM image of the InAs/Si interface, and (j) associated fast Fourier transform (FFT) revealing their epitaxial relationship and differences in lattice parameters. (k,l) Low-magnification images of the region where two wings merge. (m,n) HRTEM image of the merging area exhibiting a perfect zinc blende crystalline structure, as shown by the corresponding diffraction pattern in (n).

150 nm long. This seed could eventually be used in the future to nucleate nanostructures growing in the (001) directions on a silicon substrate.

Internal Crystal Structure of the V-Shaped Nanomembrane and Its Nucleus. Interface and Polarity. Having determined the general morphology of the V-shaped nanomembranes, growth directions, and epitaxial relationship with respect to the substrate, we now turn to their detailed internal crystal structure. Figure 1h shows low-resolution TEM micrographs of the base of the InAs nanostructures grown at 520 °C, 1.15×10^{-5} As_4 Torr, and In nominal rate of 0.2 Å/s. The first distinguishing feature is the presence of the two arms extending from a central base. A small "foot" is clearly visible in the center of the V-shape, which corresponds to the part of the membrane forming the interface with the Si substrate (Figure 3c). This foot has the same dimensions as the hole diameter in the SiO_2 mask (80 nm long and 20 nm thick). Interestingly, we find a triangular island (nucleus) at the central part of the structure. From this point, the two arms grow in a ≈19° angle consistent with the ⟨111⟩ direction of the substrate. The wings are flat with a slightly triangular shape. The flat facets correspond to the low-energy nonpolar (0−11) and (01−1) surfaces. A similar nucleation stage was observed in the case of tetrapod formation in other material systems, although only connected to the substrate *via* van der Waals interactions in those cases.[17]

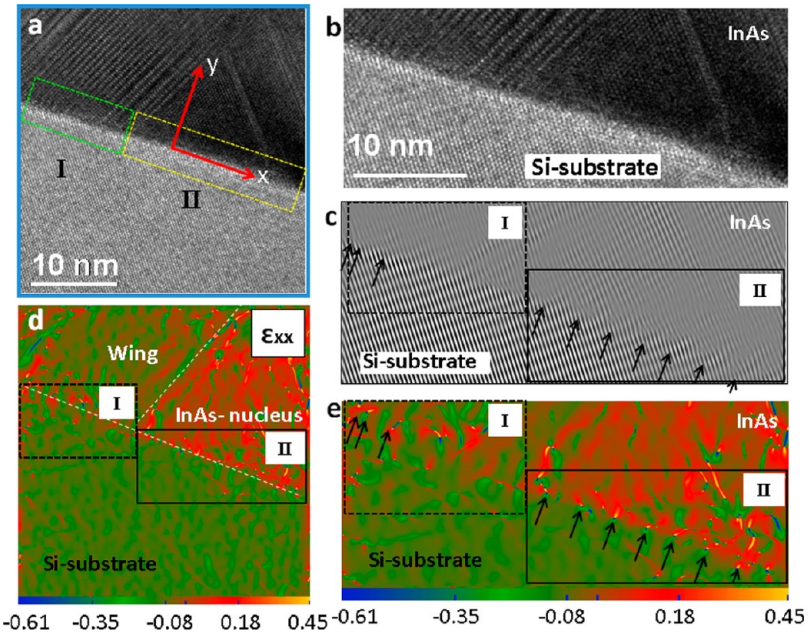

Figure 2. (a,b) Detail on the cross-sectional high-resolution TEM images taken at the interface between the InAs V-shaped nanomembrane and the Si substrate. Regions corresponding to the pyramidal nucleus and the V-shaped membrane are marked, respectively, with a yellow (II) and green (I) square. (c) Inverse Fourier transformation image obtained by masking (11−1), which enables the visualization of the dislocations (marked with arrows). The distance between dislocations at the pyramidal island level is about 2.5 ± 2 nm, while they become more sporadic in the region of the V-shaped membrane. (d,e) Strain maps estimated from image in (a). The arrows in (c) indicate the position of local strain.

The nature of the interface between the InAs and the silicon is important for applications in which the membranes should be linked electronically with the substrate. A typical HRTEM image of the interface is shown in Figure 2a,b. We distinguish two regions, corresponding (I) to the V-shaped membrane and (II) to the pyramidal nucleus. The mismatch between InAs and Si is 11.6%, meaning that the accommodation should create some misfit dislocations, as observed in the case of nanowires grown on Si. We have filtered the image from Figure 2a by selecting the diffraction spots (11−1) from InAs and Si in order to determine the possible existence of misfit dislocations. This is shown in Figure 2c. We indicate with arrows the positions where a misfit dislocation appears, shown by the discontinuity between the planes from Si to InAs. In the pyramidal region of the sample, dislocations are separated by about 2.5 ± 2 nm, in agreement with what was obtained by other groups with InAs nanowires on Si. Interestingly, the presence of dislocations in the region outside the pyramidal nucleus becomes more random and sporadic. We believe this is a consequence from the growth mechanism: the InAs nucleus grows directly on the Si substrate, while the wings grow/form directly on the facets of the pyramid. This is further supported by the strain analysis shown in Figure 2d,e. The pyramidal nucleus and the wings of the membrane exhibit a clearly different strain. In fact, the wings appear to be relatively relaxed, while the nucleus is highly strained.

A low-resolution HRTEM of a typical V-shaped membrane is shown in Figure 3a−c. The two wings are separated by a grain boundary at the interface, as can be seen in Figure 3b,c. Stripes of different contrast are observed along the two arms perpendicular to the growth direction, indicating the presence of planar defects, discussed further in the following. Because silicon is a nonpolar semiconductor, whereas III−V semiconductors are polar, it is of interest to evaluate the polarity of the membranes. Convergent beam electron diffraction (CBED) was used for this purpose. The CBED patterns are shown in Figure 3d with the corresponding computer-simulated pattern used for confirming the interpretation. By comparing the simulated CBED pattern with the measured one, we confirm that the growth direction is along the [000−1] direction, indicating that both arms grow with a B polarity (group-V-terminated). This procedure was repeated for several nanowings, and in every case, we found the growth direction to be [000−1].

As it has been shown above, HRTEM micrographs of the interface of the membranes with the substrate reveal that the nucleus of the structure consists of a triangle defined by a (100) bottom facet and two (11−1) and (1−11) inclined facets (Figure 4a). The triangle crystal structure is pure zinc blende, as confirmed by the diffractogram (Figure 4b). Figure 4c corresponds to an atomic force microscopy (AFM) measurement of a nucleus obtained after 5 min of growth. A truncated pyramid with the facets parallel to the directions ⟨011⟩ and ⟨0−11⟩ is observed. The flat top of the pyramid contrasts with the perfect triangular shape observed in HRTEM. Now the question is what

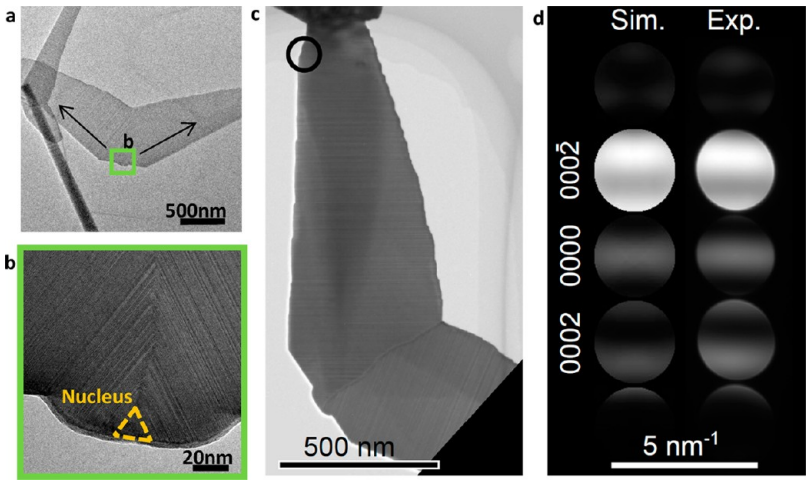

Figure 3. (a,b) TEM micrograph of a typical V-shaped InAs nanostructure. All the V-shaped InAs nanostructures analyzed exhibit distinguishing features: a nucleus region in the base and two arms coming out of this nucleus. (c) Bright-field TEM image of an arm of the V-shaped InAs nanostructures; (d) experimental and simulated ⟨14−50⟩ CBED patterns of the arm, respectively. CBED patterns were simulated for thicknesses of 30−150 nm with the JEMS software, and the best match was selected (in this case 45 nm).

the relation between the orientation of the nucleus and that of the membrane with respect to the substrate is.

In order to provide some insight on the possible orientation mechanisms of the membranes on the substrate, the initial stages of growth are discussed from the atomistic point of view: atomic models are constructed to illustrate the epitaxy between the InAs island and the Si(001) surface. A top view of this model showing a pyramidal seed oriented in the two [011] zone axes is shown in Figure 4d. The atomic modeling of the interface between the InAs pyramidal seed and the Si substrate needs to consider two elements: (i) the structure of the Si(100) formed by terraces (implying the presence of single or double steps) and (ii) the polarity of the interface between the seed and the substrate, being B or A depending if As or In atoms are the ones bonding directly with the Si substrate, respectively. The role of the Si surface structure and polarity is illustrated in Figure 5, where we sketch the cross section of the four types of structures cutting along a ⟨011⟩ direction.

Figure 5a,b illustrates the atomic configuration of As and In atoms on a silicon surface. In the cross section along the (011) planes of diamond and zinc blende structure, the atoms typically arrange in hexagons, forming a honeycomb network. Depending on where the Si(100) surface is cut, we have two types of configurations of the Si surface, as shown in Figure 5a,b. Other reports have shown that the two surface atomic configurations exist and that the surface is composed of terraces with one or the other configuration.[51−53] The oxide formation and subsequent removal in perfectly flat Si(100) also results in the creation of terraces.[54] The two configurations are related by a 90° rotation. Now, we consider at the atomic arrangement of the base of the InAs pyramid, arbitrarily fixing the interface as As−Si (A polarity of the interface). This is illustrated in Figure 5a,b. For each type of Si terrace, only one configuration of the InAs island is possible: the one that allows the completion of the hexagon, as indicated in Figure 5a,b. This determines the relative orientation of the facets of the pyramid being B polar, which are the ones enabling the fast membrane growth. As a consequence, the (111)B facets of the islands (and the membranes) will be oriented in one [011] direction or rotated by 90° depending on the type of terrace they start growing on. A similar effect is observed if one considers that the interface is formed by As−Si bonds (A polarity at the interface), as illustrated in Figure 4c,d. In this case, the direction of the B polar facets will just be rotated by 90° with respect to the precedent one. The fact that the ratio between the two membrane orientations is about 50%, under the growth conditions detailed in the Methods section, lets us suspect almost all of the seeds may have the same polarity. In the case of GaAs nanowire growth on Si(111), however, the two polarities (A and B) at the interface have been observed on the same sample.[55] Furthermore, it has been shown that certain growth conditions influence in a deterministic manner the polarity at the interface with the substrate.[56,57] In our case, it will be necessary to perform statistical measurements of the seed polarity, obtained with a large set of different growth conditions, before one can confirm the prevalence of one scenario over the other.

The nucleation and growth of the InAs membranes may occur as follows. InAs growth is performed under temperature and flow conditions such that adatoms only incorporate in the areas of the substrate without oxide.[58] In the initial stages of growth, InAs grows epitaxially on the open Si openings of the mask. Following the theory of Stranski−Krastanov quantum dot formation, one can speculate that a defect-free pyramidal-shaped island should form after the deposition

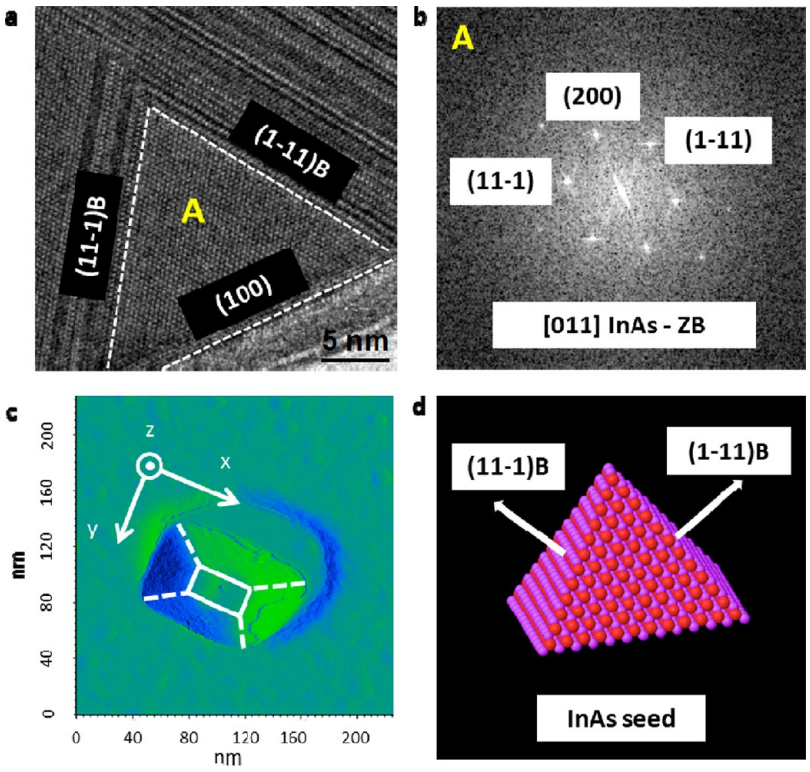

Figure 4. (a) HRTEM of the nucleus, indicating the interface with the substrate Si(100) and the membrane wings. (b) Power spectrum of the nucleus indicating zinc blende structure, (c) atomic force micrograph of the nucleus obtained after 5 min growth and the corresponding atomistic model in (d).

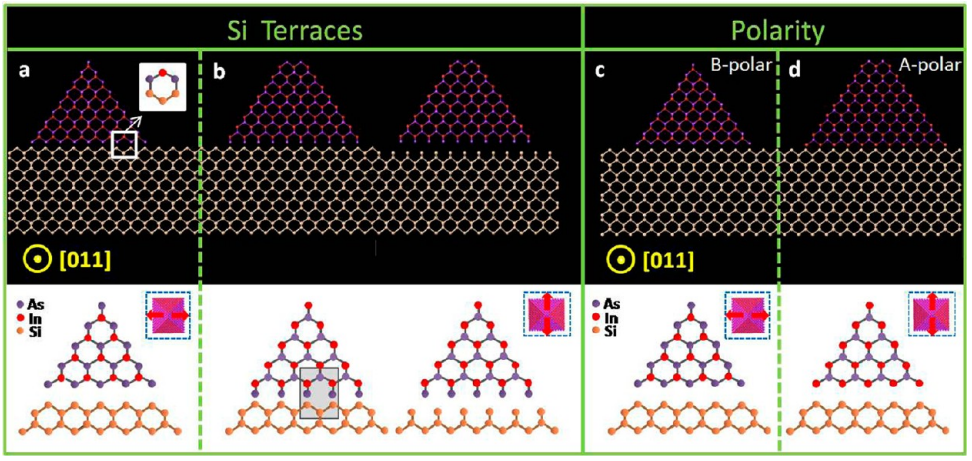

Figure 5. Atomistic model of the coupling between the [001] Si substrate and the InAs pyramid. The orange spheres represent Si atoms, while the blue and red represent, respectively, As and In. The coupling of the Si terrace with the InAs island depends on the type of termination on both sides of the interface. We plot the possible configurations depending on the type of Si terrace and polarity of the seed.

of 1 ML of InAs. This pyramid would be bound by low index surfaces to minimize its total surface free energy, in agreement with the {111} facets observed in this work. Subsequently, growth would proceed selectively on the two (111)B facets of the pyramid. On the two opposite {110} planes of the membrane, nucleation is relatively slow compared to the following step-flow, hence birth-and-spread growth mode is favored, and lateral growth takes the form of complete layers, explaining the absence of tapering (homogeneous thickness).

Light-Scattering Experiments and Electromagnetic Modeling. The light-scattering and localization properties of metal–dielectric nanostructures have recently attracted considerable attention due to the possibility of engineering light–matter coupling at the nanoscale for a number of nanophotonic device applications.[59,60] In particular, the shape-dependent resonances of conduction electrons in metallic nanostructures, known as nanoplasmonic resonances, are widely investigated for their ability to concentrate electromagnetic fields over

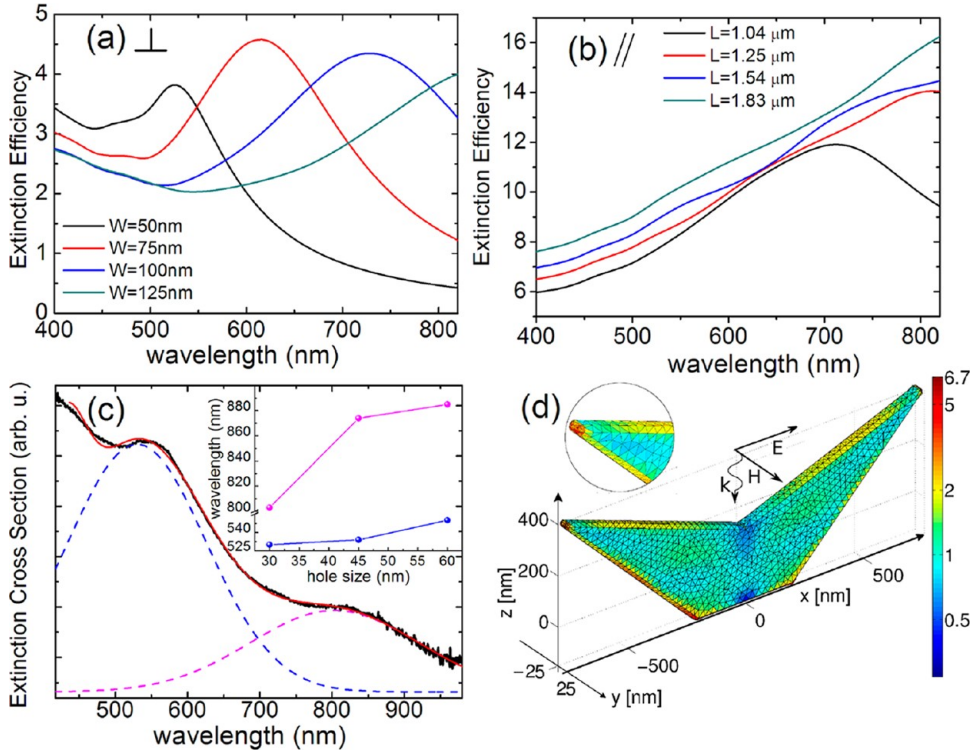

Figure 6. (a) Extinction efficiency spectrum for an isolated nanowing with fixed length $L = 1.54\ \mu$m and for varying width W, excited by a plane wave propagating in the direction of the negative z-axis and polarized along y (transverse to the V, see panel d for the reference system). (b) Extinction efficiency for a nanowing with fixed width $W = 50$ nm and for varying length L, excited by a plane wave polarized along x (parallel to the V). (c) Scattering cross section as a function of the wavelength. The experimental spectrum has been fitted by two Gaussian line shapes (dotted lines), and their sum (red continuous line) is compared with the experimental data (black continuous line). (Inset) Peak wavelength of the two peaks extracted from the experimental data as a function of the hole size. (d) Distribution of the magnitude of the electric field calculated at $\lambda = 800$ nm (in logarithmic scale) on the surface of a nanowing with $L = 1.54$ and $W = 50$ nm excited by a plane wave polarized along x. In the inset of panel d, a zoom of the field distribution in proximity to the left corner is reported.

subwavelength regions, leading to significant electric field enhancement at the nanoscale. Moreover, resonant light scattering by nanoscale structures with high refractive index can also lead to largely tunable optical resonances in purely dielectric materials.[61−63] However, this approach is currently limited to the engineering of Mie scattering resonances in highly regular nanostructures, such as semiconductor nanowires, which offer great spectral tunability but only limited local field concentration.

The control of dielectric nanostructures with highly asymmetric shapes and irregular geometries featuring sharp tips, such as the ones demonstrated by V-shaped membranes, provides a largely tunable approach for the engineering of strongly confined resonant fields on Si. In the following, we investigate the distinctive light-scattering properties of these novel dielectric nanostructures using a highly accurate formulation of the surface integral equation (SIE) method.[49] Further details on the calculations are discussed in the Methods section.

In Figure 6a,b, we show the calculated wavelength spectra of the extinction efficiencies for a representative nanowing structure normally excited by a monochromatic plane wave with electric field polarization either perpendicular (Figure 6a) or parallel (Figure 6b) with respect to the $x-z$ axis shown in Figure 6d. The results in Figure 6a correspond to structures with different widths W and a constant length $L = 1.54\ \mu$m, as defined in Figure 6d. A clear resonant behavior, controlled by the thickness of the wall, is predicted for the scattering of the transverse excitation mode of the structure. These resonances gradually red shift by increasing the wall thickness. In the case of parallel excitation in Figure 6b, we obtain a similar resonant scattering behavior but shifted to longer wavelengths, consistently with the significantly larger polarizability probed along this polarization direction, resulting in the excitation of a longitudinal mode in the structure. In Figure 6b, the results are shown for different lengths of the walls, while keeping the thickness fixed at 50 nm.

In Figure 6c, we show the experimentally measured extinction spectrum of the nanowing structure excited by incoherent white illumination, which demonstrates the presence of the two well-defined resonances theoretically predicted and corresponding to the longitudinal and transverse modes of the structure. Moreover, the peak positions of the experimentally measured modes red shift by increasing the size of the nanowing structures, as demonstrated by the inset of Figure 6c

for a number of investigated structures. The spectral positions and the line shapes (obtained by Gaussian deconvolution) of these two modes have also been found to be in good agreement with our theoretical predictions. However, we notice that the experimental dark-field excitation conditions introduce a spectral broadening with respect to the theoretical spectra, which are calculated under normal incidence illumination.[64,65] Therefore, the agreement between the measured and calculated spectra, though well capturing all of the relevant features of the experimental scattering behavior of V-shaped membranes, should be considered only qualitatively. Finally, in Figure 6d, we plot the calculated electric field distribution on the surface of the nanowing structure, best representing the one measured in Figure 6c, at the resonant longitudinal frequency. The ability of the fabricated nanostructures to localize and to significantly enhance (*i.e.*, by over a factor of 6) the electric field at the tips of the nanowing is clearly demonstrated by Figure 6d. The highly tunable scattering response of the fabricated nanowing structures along with their ability to significantly localize and enhance electromagnetic radiation at controllable tip locations can provide an alternative approach for the manipulation of nanoscale optical fields on a Si substrate for a number of device applications, such as tip-enhanced nanosensors, light emitters, and nonlinear optical elements in a purely dielectric platform.

CONCLUSIONS

In conclusion, we have reported on a new form of III−V compound semiconductor nanostructures growing epitaxially as vertical V-shaped membranes on Si[001]. Precise position control of the InAs nanostructures in regular arrays has been demonstrated by bottom-up synthesis using molecular beam epitaxy in nanoscale apertures on a SiO_2 mask. The InAs V-shaped nanomembranes originate from the two opposite facets of a rectangular pyramidal island nucleus. At the same time, when the tip of the membranes merge, we observe the formation of a relatively large defect-free zinc blende island developing in the [001] direction. By tuning growth parameters and pattern geometry, the nanomembranes can be engineered to connect and thus create controllable hierarchical structures. We also determined the presence of distinctive shape-dependent optical resonances significantly enhancing the local intensity of incident electromagnetic fields over tunable spectral regions. These V-shaped nanomembrane structures have an interesting potential in applications as nanosensors, infrared light emitters, and nonlinear optical elements.

METHODS

Growth. The InAs membranes were synthesized by molecular beam epitaxy in a DCA P600 system. Growth has been performed on patterned ⟨100⟩ p-doped silicon wafers with cut off of $0 \pm 0.5°$ and a resistivity of 0.1−0.5 Ωcm. The growth mask consisted of a 20 nm thick SiO_2 layer of thermal oxide, which was patterned following typical nanofabrication methods as reported elsewhere.[45,66,67] Special care was taken to ensure a perfectly clean and oxide-free surface in the holes. Prior to the introduction to the MBE reactor, we performed a 2 s dip in a solution of buffered HF (BHF, 7:1) and kept the sample in isopropyl alcohol until it was introduced in the load lock. The substrates were subsequently degassed at 600 °C for 2 h. Just before the growth, they were heated to 770 °C for 30 min to further remove possible surface contaminants. The growth was carried out at a nominal In growth rate of 0.2 Å/s, As_4 partial pressure between 0.8 and 1.15×10^{-5} Torr, at a temperature between 500 and 520 °C, and with 7 rpm rotation.

Electron Microscopy. To analyze the crystalline structure of the InAs membranes, we used a Phillips CM300 electron microscope operated at 300 kV from the Centre Interdisciplinaire de Microscopie Électronique (CIME) at EPFL Lausanne. For the determination of the polarity of the same membranes, we used the JEOL 3000F electron microscope at n-CHREM at Lund University, operating in TEM mode at 300 kV. CBED patterns were acquired in the wurtzite ⟨14−50⟩ zone axis and compared to patterns simulated by the Bloch wave method in JEMS. The ⟨14−50⟩ zone axis was chosen due to the clear asymmetric contrast in the (0002) and (000−2) discs and since it requires less tilt from the preferred ⟨11−20⟩ orientation of the nanowings than the alternative ⟨1−100⟩.

A perpendicular TEM lamella was prepared by standard means, using focused ion beam and a micromanipulator on protected as-grown V-shaped membranes, specifically to obtain information about the epitaxial relationship with the substrate. For all other analyses, we performed the simple sample preparation, where the InAs membranes were mechanically transferred to a holey carbon grid, to be then studied with the two electron microscopes.

Optical Scattering Measurements. Optical scattering measurements were performed under incoherent white light illumination (broad-band halogen lamp) using a custom-made dark-field microscope set up with a 50× long-working distance objective (NA = 0.75), and spatial filtering at the detector was used for background noise reduction. Scattered light was collected into a fiber-coupled CCD spectrometer (Ocean Optics QE65000). The same setup was used also for imaging and aligning the sample in order to ensure overlap between the illuminated area and the patterned structures. For this purpose, the output of the objective was sent also to a camera sensitive to visible light (Apogee Alta U4000 camera w/KAI-4022 CCD). All of the scattering spectra were background-corrected with respect to the normalized emission line shape of the excitation lamp, the detector sensitivity, and the system's collection efficiency.

Electromagnetic Simulation. Electromagnetic scattering calculations were performed according to a recently developed SIE method. The integral formulations of the Maxwell equations were very effective to treat the scattering from large arbitrary shaped particles since they require only the discretization of the spatial domain occupied by the scatterers, while the radiation conditions at infinity are naturally satisfied. In particular, the surface integral equations (SIE), which are based on the equivalent theorem for the electromagnetic fields, only require a discretization of the surface of the scatterers. Some of the most widely used SIE formulations are the PMCHWT (Poggio, Miller, Chang, Harrington, and Wu) formulation,[68] and the null field method (NFM).[69] Only in the past few years, those methods have been applied to the electromagnetic scattering by plasmonic nanostructures. In particular, the PMCHWT formulation has been investigated by Kern and Martin,[70] while the NFM has been studied in ref 71. A detailed comparison between several SIE formulations has been performed in ref 48, where their

convergence rate and accuracy have been carefully addressed. In this paper, we solve the PMCHWT with Rao Wilton Glisson (RWG) basis functions. In each of the SIE calculations presented in this work, more than 10k degrees of freedom have been used to numerically solve the scattering problem.

Conflict of Interest: The authors declare no competing financial interest.

Acknowledgment. The authors thank funding from ERC through grant UpCon, and SNF funding through Grants 121758/1 and 129775/1/and the NCCR QSIT. S.C.B. thanks the Marie Heim-Vögtlin program of SNF. L.D.N. thanks funding from International Division of SNF. This work was partly supported by the AFOSR under Award FA9550-10-1-0019, by the NSF Career Award No. ECCS-0846651, and by the U.S. Army Research Laboratory through the Collaborative Research Alliance (CRA) for MultiScale multidisciplinary Modeling of Electronic materials (MSME). A.F.i.M. and A.D.M. thank A. Kis for technical support with the AFM.

REFERENCES AND NOTES

1. Hu, J. T.; Odom, T. W.; Lieber, C. M. Chemistry and Physics in One-Dimension: Synthesis and Properties of Nanowires and Nanotubes. *Acc. Chem. Res.* **1999**, *32*, 435–445.
2. Gudiksen, M. S.; Lauhon, L. J.; Wang, J.; Smith, D. C.; Lieber, C. M. Growth of Nanowire Superlattice Structures for Nanoscale Photonics and Electronics. *Nature* **2002**, *415*, 617–620.
3. Caroff, P.; Dick, K. A.; Johansson, J.; Messing, M. E.; Deppert, K.; Samuelson, L. Controlled Polytypic and Twin-Plane Superlattices in III–V Nanowires. *Nat. Nanotechnol.* **2009**, *4*, 50–55.
4. Liu, J. P.; Huang, X.; Li, Y. Y.; Sulieman, K. M.; He, X. Hierarchical Nanostructures of Cupric Oxide on a Copper Substrate: Controllable Morphology and Wettability. *J. Mater. Chem.* **2006**, *16*, 4427–4434.
5. Cheng, W.; Campolongo, M. J.; Tan, S. J.; Luo, D. Free-standing Ultrathin Nano-membranes *via* Self-Assembly. *Nano Today* **2009**, *4*, 482–493.
6. Arzt, E.; Gorb, S.; Spolenak, R. From Micro to Nano Contacts in Biological Attachment Devices. *Proc. Natl. Acad. Sci. U.S.A.* **2003**, *100*, 10603–10606.
7. Hiramatsu, M.; Shiji, K.; Amano, H.; Hori, M. Fabrication of Vertically Aligned Carbon Nanowalls Using Capacitively Coupled Plasma-Enhanced Chemical Vapor Deposition Assisted by Hydrogen Radical Injection. *Appl. Phys. Lett.* **2004**, *84*, 4708–4710.
8. Vendamme, R.; Onoue, S. Y.; Nakao, A.; Kunitake, T. Robust Free-Standing Nanomembranes of Organic/Inorganic Interpenetrating Networks. *Nat. Mater.* **2006**, *5*, 494–501.
9. Aagesen, M.; Johnson, E.; Sorensen, C. B.; Mariager, S. O.; Feidenhans'l, R.; Spiecker, E.; Nygard, J.; Lindelof, P. E. Molecular Beam Epitaxy Growth of Free-Standing Plane Parallel InAs Nanoplates. *Nat. Nanotechnol.* **2007**, *2*, 761–764.
10. Guo, C. F.; Zhang, J.; Tian, Y.; Liu, Q. A General Strategy to Superstructured Networks and Nested Self-Similar Networks of Bismuth Compounds. *ACS Nano* **2012**, *6*, 8746–8752.
11. Dick, K. A.; Deppert, K.; Larsson, M. W.; Martensson, T.; Seifert, W.; Wallenberg, L. R.; Samuelson, L. Synthesis of Branched 'Nanotrees' by Controlled Seeding of Multiple Branching Events. *Nat. Mater.* **2004**, *3*, 380–384.
12. Zhang, H.; Cao, G. P.; Wang, Z. Y.; Yang, Y. S.; Shi, Z. J.; Gu, Z. N. Growth of Manganese Oxide Nanoflowers on Vertically-Aligned Carbon Nanotube Arrays for High-Rate Electrochemical Capacitive Energy Storage. *Nano Lett.* **2008**, *8*, 2664–2668.
13. Li, Y. B.; Bando, Y.; Golberg, D. MoS_2 Nanoflowers and Their Field-Emission Properties. *Appl. Phys. Lett.* **2003**, *82*, 1962–1964.
14. Fan, H. J.; Werner, P.; Zacharias, M. Semiconductor Nanowires: From Self-Organization to Patterned Growth. *Small* **2006**, *2*, 700–717.
15. Morales, A. M.; Lieber, C. M. A Laser Ablation Method for the Synthesis of Crystalline Semiconductor Nanowires. *Science* **1998**, *279*, 208–211.
16. Dayeh, S. A.; Yu, E. T.; Wang, D. III–V Nanowire Growth Mechanism: V/III, Ratio and Temperature Effects. *Nano Lett.* **2007**, *7*, 2486–2490.
17. Utama, M. I. B.; Zhang, Q.; Jia, S. K.; Li, D.; Wang, J.; Xiong, Q. Epitaxial II–VI Tripod Nanocrystals: A Generalization of van der Waals Epitaxy for Nonplanar Polytypic Nanoarchitectures. *ACS Nano* **2012**, *6*, 2281–2288.
18. Manna, L.; Scher, E. C.; Alivisatos, A. P. Synthesis of Soluble and Processable Rod-, Arrow-, Teardrop-, and Tetrapod-Shaped CdSe Nanocrystals. *J. Am. Chem. Soc.* **2000**, *122*, 12700–12706.
19. Dick, K. A.; Deppert, K.; Karlsson, L. S.; Seifert, W.; Wallenberg, L. R.; Samuelson, L. Position-Controlled Interconnected InAs Nanowire Networks. *Nano Lett.* **2006**, *6*, 2842–2847.
20. Tian, B. Z.; Xie, P.; Kempa, T. J.; Bell, D. C.; Lieber, C. M. Single Crystalline Kinked Semiconductor Nanowire Superstructures. *Nat. Nanotechnol.* **2009**, *4*, 824–829.
21. Musin, I. R.; Filler, M. A. Chemical Control of Semiconductor Nanowire Kinking and Superstructure. *Nano Lett.* **2012**, *12*, 3363–3368.
22. Rauber, M.; Alber, I.; Müller, S.; Neumann, R.; Picht, O.; Roth, C.; Schökel, A.; Toimil-Molares, M. E.; Ensinger, W. Highly-Ordered Supportless Three-Dimensional Nanowire Networks with Tunable Complexity and Interwire Connectivity for Device Integration. *Nano Lett.* **2011**, *11*, 2304–2310.
23. Jiang, Z.; Qing, Q.; Xie, P.; Gao, R.; Lieber, C. M. Kinked p–n Junction Nanowire Probes for High Spatial Resolution Sensing and Intracellular Recording. *Nano Lett.* **2012**, *12*, 1711–1716.
24. Tian, B.; Cohen-Karni, T.; Qing, Q.; Duan, X.; Xie, P.; Lieber, C. M. Three-Dimensional, Flexible Nanoscale Field Effect Transistors as Localized Bioprobes. *Science* **2010**, *329*, 830–834.
25. Gudiksen, M. S.; Lauhon, L. J.; Wang, J.; Smith, D. C.; Lieber, C. M. Growth of Nanowire Superlattice Structures for Nanoscale Photonics and Electronics. *Nature* **2002**, *415*, 617–620.
26. Samuelson, L.; Thelander, C.; Björk, M. T.; Borgström, M.; Deppert, K.; Dick, K. A.; Hansen, A. E.; Martensson, T.; Panev, N.; Persson, A. I.; Seifert, W.; Sköld, N.; Larsson, M. W.; Wallenberg, L. R. Semiconductor Nanowires for 0D and 1D Physics and Applications. *Physica E* **2004**, *25*, 313–318.
27. Wright, S. L.; Inada, M.; Kroemer, H. Polar-on-Nonpolar Epitaxy: Sublattice Ordering in the Nucleation and Growth of GaP on the Si(113) Surface. *J. Vac. Sci. Technol.* **1982**, *21*, 534.
28. Bessire, C. D.; Björk, M. T.; Schmid, H.; Schenk, A.; Reuter, K. B. Trap-Assisted Tunneling in Si–InAs Nanowire Heterojunction Tunnel Diodes. *Nano Lett.* **2011**, *11*, 4195–4199.
29. Samuelson, L.; Ohlsson, J.; Martensson, T.; Svenson, P. Nanowire Growth on Dissimilar Material. Patent Appl. 20120145990, June 14, 2012.
30. Biermanns, A.; Breuer, S.; Trampert, A.; Davydok, A.; Geelhaar, L.; Pietsch, U. Strain Accommodation in Ga-Assisted GaAs Nanowires Grown on Silicon (111). *Nanotechnology* **2012**, *23*, 305703–305711.
31. Shin, J. C.; Kim, K. H.; Yu, K. J.; Hu, H.; Yin, L.; Ning, C.-Z.; Rogers, J. A.; Zu, J-M; Li, X. $InxGa_{1-x}As$ Nanowires on Silicon: One-Dimensional Heterogeneous Epitaxy, Bandgap Engineering, and Photovoltaics. *Nano Lett.* **2011**, *11*, 4831–4838.
32. Kroemer, H. Polar-on-Nonpolar Epitaxy. *J. Cryst. Growth* **1987**, *81*, 193–204.
33. Kwon, O.; Boeckl, J. J.; Lee, M. L.; Pitera, A. J.; Fitzgerald, E. A.; Ringel, S. A. Monolithic Integration of AlGaInP Laser Diodes on SiGe/Si Substrates by Molecular Beam Epitaxy. *J. Appl. Phys.* **2006**, *100*, 013103–013110.
34. Huang, S. H.; Balakrishnan, G.; Khoshakhlagh, A.; Dawson, L. R.; Huffaker, D. L. Simultaneous Interfacial Misfit Array Formation and Antiphase Domain Suppression on Miscut Silicon Substrate. *Appl. Phys. Lett.* **2008**, *93*, 071102–071105.
35. Reboul, J. R.; Cerutti, L.; Rodriguez, J. B.; Grech, P.; Tournié, E. Continuous-Wave Operation above Room Temperature of GaSb-Based Laser Diodes Grown on Si. *Appl. Phys. Lett.* **2011**, *99*, 121113–121116.

36. Desplanque, L.; El Kazzi, S.; Coinin, C.; Ziegler, S.; Kunert, B.; Beyer, A.; Volz, W.; Wang, Y.; Ruterana, P.; Wallart, X. Monolithic integration of high electron mobility InAs-based heterostructure on exact (001) Silicon using a GaSb/GaP accommodation layer. *Appl. Phys. Lett.* **2012**, *101*, 142111.
37. Tong, Q. Y.; Gösele, U. Semiconductor Wafer Bonding: Recent Developments. *Mater. Chem. Phys.* **1994**, *37*, 101–127.
38. Fontcuberta i Morral, A.; Zahler, J. M.; Atwater, H. A.; Ahrenkiel, S. P.; Wanlass, M. W. InGaAs/InP Double Heterostructures on InP/Si Templates Fabricated by Wafer Bonding and Hydrogen-Induced Exfoliation. *Appl. Phys. Lett.* **2003**, *83*, 5413–5415.
39. Hong, J. M.; Wang, S.; Sands, T.; Washburn, J.; Flood, J. D.; Merz, J. L.; Low, T. Selective-Area Epitaxy of GaAs through Silicon Dioxide Windows by Molecular Beam Epitaxy. *Appl. Phys. Lett.* **1986**, *48*, 142–144.
40. Mohan, P.; Motohisa, J.; Fukui, T. Controlled Growth of Highly Uniform, Axial/Radial Direction-Defined, Individually Addressable InP Nanowire Arrays. *Nanotechnology* **2005**, *16*, 2903–2907.
41. Tomioka, K.; Yoshimura, M.; Fukui, T. A III−V Nanowire Channel on Silicon for High-Performance Vertical Transistors. *Nature* **2012**, *488*, 189–192.
42. Shimizu, T.; Xie, T.; Nishikawa, J.; Shingubara, S.; Senz, S.; Gösele, U. Synthesis of Vertical High-Density Epitaxial Si(100) Nanowire Arrays on a Si(100) Substrate Using an Anodic Aluminum Oxide Template. *Adv. Mater.* **2007**, *19*, 917–920.
43. Wang, J.; Plissard, S.; Hocevar, M.; Vu Thuy, T. T.; Zehender, T.; Immink, G. W.; Verheijen, M. A.; Haverkort, J.; Bakkers, E. P. A. M. Position-Controlled [100]InP Nanowire Arrays. *Appl. Phys. Lett.* **2012**, *100*, 053107–053110.
44. Tomioka, K.; Motohisa, J.; Hara, S.; Fukui, T. Control of InAs Nanowire Growth Directions on Si. *Nano Lett.* **2008**, *8*, 3475–3480.
45. Plissard, S.; Larrieu, G.; Wallart, X.; Caroff, P. High Yield of Self-Catalyzed GaAs Nanowire Arrays Grown on Silicon *via* Gallium Droplet Positioning. *Nanotechnology* **2011**, *22*, 275602.
46. Dimakis, E.; Lahnemann, J.; Jahn, U.; Breuer, S.; Hilse, M.; Geelhaar, L.; Riechert, H. Self-Assisted Nucleation and Vapor−Solid Growth of InAs Nanowires on Bare Si(111). *Cryst. Growth Des.* **2011**, *11*, 4001–4008.
47. Hertenberger, S.; Rudolph, D.; Bichler, M.; Finley, J. J.; Abstreiter, G.; Koblmüller, G. Growth Kinetics in Position-Controlled and Catalyst-Free InAs Nanowire Arrays on Si(111) Grown by Selective Area Molecular Beam Epitaxy. *J. Appl. Phys.* **2010**, *108*, 114316.
48. Björk, M. T.; Schmid, H.; Breslin, C. M.; Gignac, L.; Riel, H. InAs Nanowire Growth on Oxide-Masked ⟨111⟩ Silicon. *J. Cryst. Growth* **2012**, *344*, 31–37.
49. Forestiere, C.; Iadarola, G.; Rubinacci, G.; Tamburrino, A.; Dal Negro, L.; Miano, G. Surface Integral Formulations for the Design of Plasmonic Nanostructures. *J. Opt. Soc. Am. A* **2012**, *29*, 2314–2327.
50. Simon, D. S.; Lawrence, N.; Trevino, J.; Dal Negro, L.; Sergienko A. V. Quantum Key Distribution with Fibonacci Orbital Angular Momentum States **2012**, http://search.arXiv.org:8081.
51. Tromp, R. M.; Hamers, R. J.; Demuth, J. E. Si(001) Dimer Structure Observed with Scanning Tunneling Microscopy. *Phys. Rev. Lett.* **1985**, *55*, 1303–1306.
52. Pukite, P. R.; Cohen, P. I. Suppression of Antiphase Domains in the Growth of GaAs on Ge(100) by Molecular Beam Epitaxy. *J. Cryst. Growth* **1987**, *81*, 214–220.
53. Narayanan, V.; Mahajan, S.; Sukidi, N.; Bachmann, K. J.; Woods, V.; Dietz, N. Orientation Mediated Self-Assembled Gallium Phosphide Islands Grown on Silicon. *Philos. Mag. A* **2000**, *80*, 555–572.
54. Döscher, H.; Kleinschmidt, P.; Hannappel, T. Atomic Surface Structure of. Si(100) Substrates Prepared in a Chemical Vapor. *Appl. Surf. Sci.* **2010**, *257*, 574.
55. Uccelli, E.; Arbiol, J.; Magen, C.; Krogstrup, P.; Russo-Averchi, E.; Heiss, M.; Mugny, G.; Morier-Genoud, F.; Nygard, J.; Morante, J. R.; Fontcuberta i Morral, A. InAs Quantum Dot Arrays Decorating the Facets of GaAs Nanowires. *Nano Lett.* **2011**, *11*, 3827–3832.
56. Tomioka, K.; Motohisa, J.; Hara, S.; Fukui, T. Control of InAs Nanowire Growth Directions on Si. *Nano Lett.* **2008**, *8*, 3475–3480.
57. Russo-Averchi, E.; Heiss, M.; Michelet, L.; Krogstrup, P.; Nygard, J.; Magen, C.; Morante, J. R.; Uccelli, E.; Arbiol, J.; Fontcuberta i Morral, A. Suppression of Three Dimensional Twinning for a 100% Yield of Vertical GaAs Nanowires on Silicon. *Nanoscale* **2012**, *4*, 1486–1490.
58. Heiss, M.; Riedlberger, E.; Spirkoska, D.; Bichler, M.; Abstreiter, G.; Fontcuberta i Morral, A. Growth Mechanisms and Optical Properties of GaAs-Based Semiconductor Microstructures by Selective Area Epitaxy. *J. Cryst. Growth* **2008**, *310*, 1049–1056.
59. Maier, S. Plasmonics: Clear for Launch. *Nat. Phys.* **2007**, *3*, 301–303.
60. Schuller, J. A.; Barnard, E.; Cai, W.; Jun, Y. C.; White, J.; Brongersm, M. L. Plasmonics for Extreme Light Concentration and Manipulation. *Nat. Mater.* **2010**, *9*, 193–204.
61. Cao, L.; White, J. S.; Park, J.-S.; Schuller, J. A.; Clemens, B. M.; Brongersm, M. L. Engineering Light Absorption in Semiconductor Nanowire Devices. *Nat. Mater.* **2009**, *8*, 643–647.
62. Cao, L.; Fan, P.; Barnard, E. S.; Brown, A. M.; Brongersma, M. L. Tuning the Color of Silicon Nanostructures. *Nano Lett.* **2010**, *10*, 2649–2654.
63. Cao, L.; Fan, P.; Vasudev, A. P.; White, J. S.; Yu, Z.; Cai, W.; Schuller, J. A.; Fan, S.; Brongersma, M. L. Semiconductor Nanowire Optical Antenna Solar Absorbers. *Nano Lett.* **2010**, *10*, 439–445.
64. Gopinath, A.; Boriskina, S.; Feng, N. N.; Reinhard, B. M.; Dal Negro, L. Photonic-Plasmonic Scattering Resonances in Deterministic Aperiodic Structures. *Nano Lett.* **2008**, *8*, 2423–2431.
65. Trevino, J.; Cao, H.; Dal Negro, L. Circularly Symmetric Light Scattering from Nanoplasmonic Spirals. *Nano Lett.* **2011**, *11*, 2008–2016.
66. Mohan, P.; Motohisa, J.; Fukui, T. Controlled Growth of Highly Uniform, Axial/Radial Direction-Defined, Individually Addressable InP Nanowire Arrays. *Nanotechnology* **2005**, *16*, 2903–2907.
67. Bauer, B.; Rudolph, A.; Soda, M.; Fontcuberta i Morral, A.; Zweck, J.; Schuh, D.; Reiger, E. Position Controlled Self-Catalyzed Growth of GaAs Nanowires by Molecular Beam Epitaxy. *Nanotechnology* **2010**, *21*, 435601–435606.
68. Mautz, J. R.; Harrington, R. F. Electromagnetic Scattering from a Homogeneous Material Body of Revolution. *Arch. Elek. Ubertragung.* **1979**, *33*, 71–80.
69. Waterman, P. C. Matrix Formulation of Electromagnetic Scattering. *Proc. IEEE* **1965**, *53*, 805–812.
70. Kern, A. M.; Martin, O. J. Surface Integral Formulation for 3D Simulations of Plasmonic and High Permittivity Nanostructures. *J. Opt. Soc. Am. A* **2009**, *26*, 732–740.
71. Forestiere, C.; Iadarola, G.; Dal Negro, L.; Miano, G. Near-Field Calculation Based on the T-Matrix Method with Discrete Sources. *J. Quant. Spectrosc. Radiat. Transfer* **2011**, *112*, 2384–2394.